JACS
JOURNAL OF THE AMERICAN CHEMICAL SOCIETY

ARTICLE

pubs.acs.org/JACS

Thermo-, Photo-, and Chemo-Responsive Shape-Memory Properties from Photo-Cross-Linked Metallo-Supramolecular Polymers

Justin R. Kumpfer and Stuart J. Rowan*

Department of Macromolecular Science & Engineering, Case Western Reserve University, 2100 Adelbert Road, Cleveland, Ohio 44106-7202, United States

Supporting Information

ABSTRACT: Films exhibiting multiresponsive shape-memory properties have been accessed using covalently cross-linked metallo-supramolecular polymers. Low molecular weight poly(butadiene) was end-capped with 4-oxy-2,6-bis(*N*-methylbenzimidazolyl)pyridine (−OMebip) ligands that upon addition of metal salts spontaneously formed high molecular weight metallo-supramolecular polymers. The addition of a tetra-functional thiol along with a photoinitiator results in mechanically stable films via solution-casting. These films consist of a soft poly(butadiene) phase and a hard metal−ligand phase. Photo-cross-linking of the poly(butadiene) soft phase, via the thiol−ene reaction, upon exposure to relatively low intensity light, allows access to a diverse range of permanent shapes. Investigations into the temporary shape fixing and recovery of these materials were undertaken to determine the effects of cross-link density and the nature of the metal salts. The key component in fixing and releasing the temporary shape is the metal−ligand hard phase, and as such any stimulus that can disrupt this phase (light, heat, or chemicals) can be used to create the temporary shape and induce its recovery back to the permanent shape.

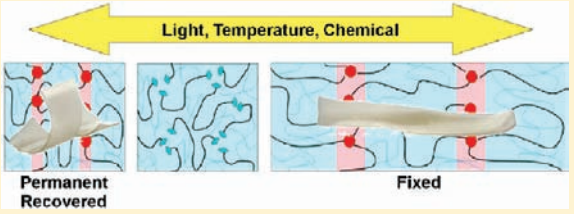

INTRODUCTION

Materials are said to exhibit shape-memory properties if they are able to fix a temporary shape and recover back to their "remembered" permanent shape when exposed to an external stimuli.[1−4] These materials typically consist of two distinct types of cross-linking: a reversible "cross-link" (usually in the form of a thermal transition such as T_g, T_m, or clearing point of a liquid crystalline material) responsible for holding the temporary shape and a nonreversible cross-link (which can be either a covalent or a physical cross-link) used to fix the permanent shape. These types of materials have gained increasing interest as a result of their many possible applications, ranging from biomedical[5−8] to textiles.[9,10]

While shape-memory effects brought about by direct heating[11−14] are the most common, other stimuli such as light[15−17] have become increasingly attractive as a consequence of the ability to utilize reduced operating temperatures, be applied remotely, and result in localized shape-memory effects.[18] Generally, light-induced shape-memory is achieved either via photochemistry or through light-induced heating. For example, Lendlein and co-workers used UV light to facilitate shape-memory effects by way of a photoreversible cycloaddition reaction.[19] Remote shape-memory effects have been developed utilizing IR irradiation[20,21] or magnetic fields[22,23] as the stimuli; however, on account of the low thermal conductivity of most polymers these materials require fillers to enhance heat transfer and facilitate the remote heating and tend not to have localized effects.

Shape-memory polymers have also been developed to be chemo-responsive.[24] Polyurethanes displaying shape-memory properties have been shown to return to their permanent states after immersion in water.[25] This results from plasticization of the polyurethanes, which decreases the polymers' T_g to below that of room temperature, upon which the samples can recover. Other solvents such as DMF, ethyl acetate, and ethyl formate have been used with the same mechanism to show shape-memory recovery of a thermosetting styrene-based resin.[26]

In this study, we report the use of supramolecular reversible cross-links, in the form metal−ligand coordination bonds,[27] as the key component that holds the material in its temporary shape, and as such we have developed a class of materials that not only respond to heat, but also to light as well as to chemicals such as methanol, acetone, and amines. The use of light here is particularly attractive as it does not require additional fillers and allows for remotely activated localized shape-memory effects. There are very few examples of shape-memory polymers that utilize noncovalent, supramolecular interactions to "fix" the temporary shape. Those that have include polyelectrolyte phase-separation,[28−31] inclusion complexes,[32] and hydrogen-bonded systems.[33−35] Work done by Anthamatten and co-workers[36] used a covalently cross-linked network that also contained the hydrogen-bonding moiety, 2-ureido-4[1*H*]-pyrimidone (UPy), as side groups. They were able to utilize the thermally sensitive hydrogen-bonded UPy dimer to achieve reversible fixing of the temporary shape. Similarly, Guan and co-workers[37] synthesized a linear polymer containing UPy groups within the polymer backbone. They found that disruption of the hydrogen bonding with

Received: June 9, 2011
Published: July 26, 2011

heating, and subsequent cooling, resulted in formation of intermolecular dimers, which imparted shape-memory properties to the films.

There is a growing amount of interest in using reversible bonds (either covalent or noncovalent) to access macroscopically responsive materials.[38−40] We and others[41,42] have recently shown that certain metal−ligand interactions are not only sensitive to heat but can also be sensitive to certain chemicals (such as nerve gas agent mimics or amines),[43,44] as well as light[45] through a photothermal conversion process. Thus, the inherent properties of the metal−ligand complexes allow for them to act as dynamic, reversible cross-links that are able to absorb UV light and transfer the energy to localized heating without the need for additional fillers. We were therefore interested in seeing if we could use such reversible metal−ligand interactions in the fixing process in shape-memory polymers. Furthermore, we were also interested in using light to form the permanent cross-links. This would then allow us to cast a film of a metallo-supramolecular polymer, process it into the desired form, and then use light to induce the covalent cross-linking and create the permanent shape.

Our proposed approach is schematically shown in Figure 1 and involves placing metal chelating ligands at the ends of a low molecular weight cross-linkable (poly(butadiene)) polymer core. The addition of a metal salt results in a metallo-supramolecular polymer where the metal−ligand complexes phase separate from the polymer core in the solid state.[45] These "hard" metal−ligand phases become the reversible cross-links in the shape memory polymer. Creation of the fixed cross-links can be achieved by the photo-cross-linking of the poly(butadiene) core with a tetra-functional thiol through a photoinduced thiol−ene reaction.[46] The metal−ligand complexes are able to absorb UV light, and this absorbed energy is converted into fluorescence and localized heating. This localized heating results in softening of the hard phase and increased decomplexation or rate of exchange of the metal−ligand complexes. Thus, the material can be deformed while exposed to UV light (or heat), and upon removal of the light the sample cools, the metal−ligand interactions re-engage, and the phase separation reforms, locking in the temporary deformed state. Further exposure to light will again break up the phase separation, and the stored strain is released and the material returns to its entropically favored, "remembered" shape. Similarly, exposure to chemicals or solvents that are able to plasticize the hard phase and/or competitively bind the metals is able to bring about shape-memory behavior.

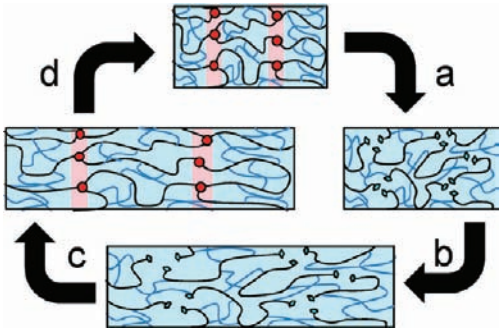

Figure 1. Proposed mechanism of shape-memory behavior using light as a stimulus: (a) UV light is absorbed by the metal−ligand complexes and is converted to localized heat, which disrupts the phase separation; (b) the material can then be deformed; (c) removal of the light while the material is deformed allows the metal−ligand complexes to reform and lock in the temporary shape; and (d) additional exposure to and subsequent removal of UV light allows for a return to the permanent shape.

EXPERIMENTAL METHODS

Materials. All solvents and reagents were purchased from Aldrich Chemical Co. and used without further purification. The hydroxyl-terminated poly(butadiene) (HTPB) was purchased from Scientific Polymer Products, Inc. with a reported M_n of 3000 g/mol and 20% cis, 20% vinyl, and 60% trans composition. All solvents were distilled with suitable drying agents, and spectroscopic grade chloroform was used to cast all films. Bistriflimide metal salts were prepared according to the literature.[47]

Instruments and Procedures. NMR spectra were recorded on a Varian 600 NMR spectrometer. Dynamic mechanical thermal analysis experiments were performed using a TA Instruments DMAQ800 under N_2 with liquid N_2 cooling and heated at a rate of 3 °C/min. UV−vis spectra were obtained on a Perkin-Elmer Lambda 800 UV−vis spectrometer. Titration experiments were performed in Quartz cuvettes scanning in the range of 250−400 nm with an integration time of 0.24 s. Molecular weights of the materials were measured by mass spectrometry on a Bruker AUTOFLEX III MALDI TOF/TOF mass spectrometer using dithranol as the matrix. The UV lamp used for photo-cross-linking and shape-memory experiments was a Bluepoint 4 Ecocure from Honle UV America Inc. All experiments were carried out with a 320−390 nm filter. Heat produced directly from the lamp was not observed to exceed 60 °C during all experiments. Small-angle X-ray scattering (SAXS) measurements were conducted using a Rigaku S-MAX 3000 SAXS system. Cu Kα X-rays from a MicroMax-002+ sealed tube source (λ = 0.154 nm) were collimated through three pinhole slits to yield a final spot size of 0.7 mm at the sample position. Two-dimensional (2D) SAXS data were collected using a Rigaku multiwire area detector with a circular active area of 133 mm and a spatial resolution of 1024 × 1024 pixels. The sample-to-detector distance and the scattering vector, q, were calibrated using a silver behenate (AgBe) standard with a characteristic (001) peak position at q = 1.076 nm^{-1}. The calculated sample-to-detector distance was 1.5 m. Typical exposure times were 1 h.

Preparation of 1. In dried glassware, 4-hydroxy-2,6-bis(10-methylbenzimidazoyl)pyridine[48] (HOMebip, 5.17 g, 14.5 mmol) and triphenylphosphine (TPP, 7.75 g, 29.5 mmol) were suspended in 75 mL of distilled THF under Ar. The suspension was cooled to ∼ −80 °C in an isopropanol−dry ice bath with stirring. To this was slowly added 7.5 mL of a 40 wt % solution of diethyl azodicarboxylate in toluene (DEAD, 34 mmol), and the reaction turned a clear, orange-brown color. In a separate flask, hydroxy-terminated poly(butadiene) (HTPB, 15.5 g, 5.2 mmol) was dissolved in 50 mL of distilled THF. The HTPB solution was added to the reaction flask at −80 °C with stirring. The reaction was left stirring for 24 h while gradually warming to room temperature. The solvent was then removed under vacuum to give a viscous oil. The product was redissolved in dichloromethane and extracted with a 1 M NaOH solution to help to remove some of the excess HOMebip, which crashes out of solution and removed by filtration. The organic fraction was washed three more times with NaOH solution, dried with Na_2SO_3, filtered, stirred with decolorizing carbon to further remove the excess HOMebip, filtered, and the solvent was removed under vacuum. The product was then purified twice by column chromatography using $CHCl_3$:MeOH, 100:0, 99:1, 98:2 to remove the remaining HOMebip and diethyl ether to remove any triphenylphosphine oxide. To remove any excess DEAD, the product was dissolved in 100 mL of dichloromethane and stirred vigorously for 3 days with 300 mL of 2 M NaOH solution. After extracting the organic layer, the solvent was removed under vacuum to give the macromonomer **1** (14.8 g, 63%). δ_H (600 MHz; $CDCl_3$) 7.93 (s, 4H, Ar), 7.852 (d, 4H, Ar), 7.44 (d, 4H, Ar),

Scheme 1. Synthesis of Metal-Chelating Ligand End-Capped Poly(butadiene) Macromonomer (1) Films That Contain Different Amounts of Tetrathiol Cross-Linker and Photoinitiator[a]

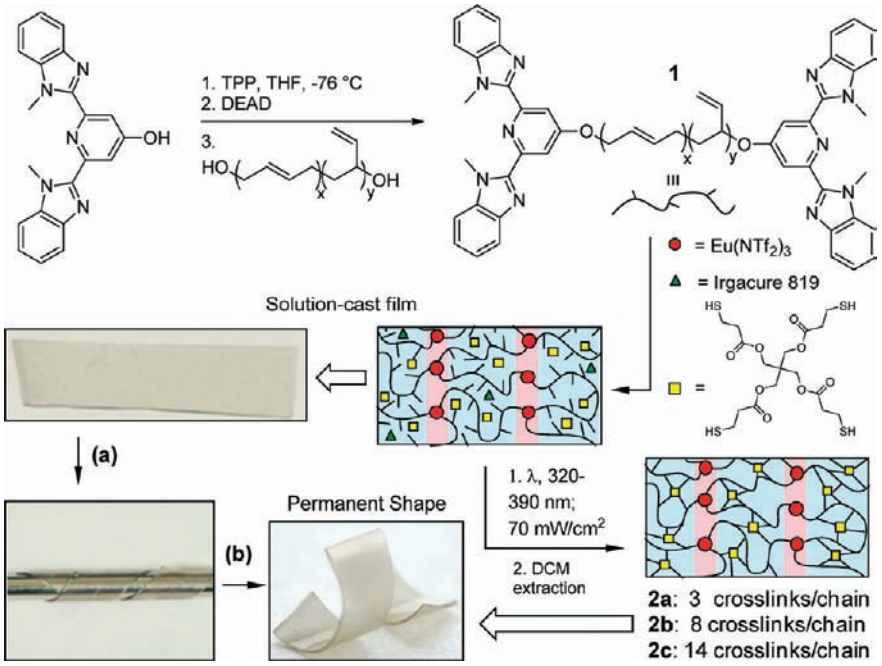

[a] Films are solution cast, and the dried films are photo-cross-linked to yield **2a**−**c**·**Eu(NTf$_2$)$_3$** with a targeted 3, 8, and 14 cross-links/chain, respectively. The solution-cast un-cross-linked films can be fixed into a variety of permanent shapes; for example, (a) a strip of un-cross-linked film is wrapped around a cylinder to give a spiral shape, and (b) irradiation with low intensity UV light initiates photo-cross-linking to yield a film with a permanent spiral shape.

7.34 (m, 8H, Ar), 5.54 (m, 14H, CH2*CH*CH), 5.39, 5.36 (m, 110H, $CH_2CHCHCH_2$), 4.95 (m, 28H, CH_2CH), 4.73 (d, 1.6H, *cis*-$CHCH_2O$), 4.22 (d, 3.2H, *trans*-$CHCH_2O$), 4.21 (s, 12H, CH_3), 4.16 (m, 1.3H, *vinyl*-$CH_2CHCHCH_2O$), 2.06 (m, 14H, CH_2CHCH_2), 2.01 (m, 220H, $CH_2CHCHCH_2$), 1.42, 1.25, (m, 28H, $CH_2CH_2CHCH_2$); δ_C (100 MHz; $CDCl_3$) 166.4, 151.3, 150.6, 142.9, 137.4, 131.5, 129.6, 128.6, 123.7, 123.0, 120.4, 114.4, 112.2, 110.1, 43.7, 38.4, 34.2, 32.9, 30.3, 27.6, 25.1. M_n = 4300 g/mol by ^{1}H NMR and UV−vis titration with $Zn(ClO_4)_2$. *m*/*z* (MALDI TOF-TOF; matrix: dithranol) M_n = 3400. PDI: 1.03.

Preparation of 2a−c·Eu(NTf$_2$)$_3$. *Typical Preparation of Metallo-Supramolecular Films.* The materials were covered with aluminum foil for all steps to prevent the polymer from photo-cross-linking before it had been cast into a film. 293 μL of Eu(NTf$_2$)$_3$ in CH_3CN (100 mM) was added to a solution of **1** (200 mg in 5 mL of $CHCl_3$), stirred for 5 min, and the solvent removed under vacuum at 40 °C to avoid potential thermal cross-linking. In a separate vial, the tetrathiol cross-linker (pentaerythritol tetrakis(3-mercaptopropionate)) and a photoinitiator (Irgacure 819) were dissolved in 4 mL of $CHCl_3$. The cross-linking density was controlled by the amount of the tetrathiol cross-linker added. Films were targeted to have 3, 8, or 14 cross-links per chain by adding 17 mg (0.035 mmol), 45.5 mg (0.093 mmol), or 79.5 mg (0.162 mmol), respectively, of the tetrathiol cross-linker and 3.0 mg (0.009 mmol), 8.7 mg (0.02 mmol), or 15.2 mg (0.04 mmol), respectively, of photoinitiator. This solution is then used to dissolve the metallo-supramolecular polymer **1**·**Eu(NTf$_2$)$_3$**. Once dissolved, the solution is cast into an aluminum walled casting dish with a Teflon sheet bottom. The solvent was allowed to evaporate at room temperature for 24 h to yield mechanically stable un-cross-linked films.

Photo-Cross-Linking of the Films. The un-cross-linked solution-cast films (at different loading of the tetrathiol cross-linker) were placed between two glass slides to avoid bending of the film. All films were irradiated using 320−390 nm light at an intensity of 70 mW/cm^2 for 1 h on each side to induce reactions of the 1,2 vinyl groups (predominantly) with the thiols. The resulting cross-linked films have gel fractions of >95% and thicknesses of 220 ± 20 μm. After the initial cross-linking, the films were exposed to higher intensity light (900−1000 mW/cm^2) to ensure maximum cross-linking. Any residual photoinitiator was removed by three extractions in dichloromethane. The resulting films **2a**−**c**·**Eu(NTf$_2$)$_3$** have targeted 3, 8, and 14 cross-links/chain, respectively.

Shape-Memory Experiments. Strips of the films with approximate dimensions of 10 mm × 5 mm × 0.2 mm were placed in the DMTA. After the initial length was recorded, the films were stretched to a set force of 1 N at 2 N/min. At the same time, the films were irradiated with UV light (320−390 nm, 900−1000 mW/cm^2). After the films reached the set force (1 N), the light was removed and the samples were allowed to equilibrate for 5 min, after which the force was removed. After we waited to observe the relaxation behavior, the films were irradiated with UV light. Experiments were performed a minimum of five times per sample to get the average values for fixing and recovery.

RESULTS AND DISCUSSION

We have previously shown that low molecular weight polymers in which a low T_g core has been end-capped with 4-hydroxy-2,6-bis(10-methylbenzimidazoyl)pyridine (HOMebip) are able to self-assemble into mechanically stable, elastomeric films when coordinated with transition metals[49] and/or lanthanides.[45] In this study, hydroxyl-terminated poly(butadiene) (HTPB) was chosen as the core polymer for its ability to be easily cross-linked through its 1,2-vinyl groups. The HTPB was end-capped with HOMebip to give a ditopic macromonomer, **1**, using the Mitsunobu reaction (Scheme 1). Following purification, the ^{1}H NMR spectrum (see Supporting Information, S1) of macromonomer **1** showed no evidence of the presence of residual

hydroxyl groups that would result from incomplete end-capping with the ligand. NMR was also used to determine the molecular weight of the macromonomer via end-group analysis, which gave M_n = 4300 g/mol. The molecular weight was further confirmed via MALDI-TOF mass spectrometry and via monitoring the UV−vis signals while titrating in $Zn(ClO_4)_2$ (see Supporting Information, S3,4).[44,48] Mechanically stable films were prepared by dissolving the macromonomer, the desired amount of the tetrathiol cross-linker, the photoinitiator, and a stoichiometric amount of metal salt to ensure full complexation (i.e., at ratios of 1:3 Eu^{3+}:ROMebip or 1:2 Zn^{2+}:ROMebip) and then solution cast. After drying, the films are photo-cross-linked using 320−390 nm UV light, and any residual photoinitiator is removed by an extraction with dichloromethane to yield the cross-linked metallo-supramolecular polymer films, **2a−c·Eu(NTf$_2$)$_3$** with a targeted 3, 8, and 14 cross-links/chain, respectively, as shown in Scheme 1.

The ability to also use light as the means of covalently cross-linking opens up the possibility of easily creating interesting and complex permanent shapes. An example of this is shown in Scheme 1, where an un-cross-linked metallo-supramolecular film was set into a permanent spiral shape by simply twisting around a substrate and irradiating with UV light. The ability to form more complex permanent shapes via photo-cross-linking should allow for uses in a wider variety of applications and devices.

Films of a metallo-supramolecular polymer made with **1** and europium bistriflimide ($Eu(NTf_2)_3$) were initially studied. We have shown previously that mechanically stable films can be formed with ditopic macromonomers based on poly(ethylene-*co*-butylene) (i.e., hydrogenated poly(butadiene)) using $La(NTf_2)_3$ as a result of phase separation of the "hard" metal−ligand complex from the "soft" polymer core.[45] Up to three terdentate ligands can bind to Eu^{3+}, and upon binding the free ligand-based emission (blue) is converted into the metal-based emission (red) of the Eu complex.[50] This occurs on account of the "antenna effect", which is in effect a light conversion process that occurs by absorption of the light by the ligand, followed by a ligand-to-metal energy transfer resulting in the metal ion-based emission. Thus, this "antenna effect" can be used to demonstrate whether the ligand is complexed to the Eu^{3+} ion (red emission) or is unbound (blue emission).[43,44,51] Europium also has a weaker binding constant with terdentate ligands than transition metals, which makes the complexes more dynamic at lower temperatures.[43]

Small angle X-ray scattering (SAXS) was used to probe the phase separation responsible for the physical, reversible cross-links and to determine the films' morphology. A representative 1D scattering plot is shown in Figure 2a for an un-cross-linked film prepared with $Eu(NTf_2)_3$ containing enough tetrathiol cross-linker and photoinitiator for a film targeting eight cross-links per chain. A primary Bragg diffraction peak corresponding to 8.70 nm is observed, which correlates to the distance between the metal−ligand "hard" phases. This value matches closely with previously published SAXS data on metallo-supramolecular films of similar molecular weight.[45] A secondary peak is also observed at 4.35 nm, one-half that of the primary peak ($2q^*$), which is typical of a lamellar morphology that we have also seen in the hydrogenated version of the material.[45]

The mechanical properties of the photo-cross-linked films **2a−c·Eu(NTf$_2$)$_3$** were investigated using dynamic mechanical thermal analysis (DMA). A control film of un-cross-linked **1·Eu(NTf$_2$)$_3$** was studied along with films of varying cross-

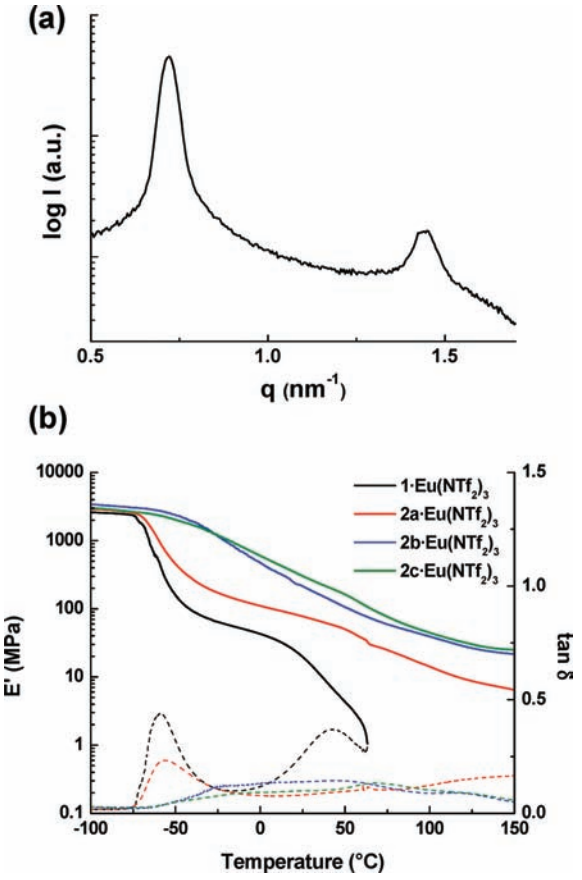

Figure 2. (a) SAXS of an un-cross-linked film of **1·Eu(NTf$_2$)$_3$** containing enough tetrathiol and photoinitiator to target eight cross-links per chain displaying a primary peak at 8.7 nm and a secondary peak of 4.3 nm, indicative of a lamellar morphology. (b) Dynamic mechanical thermal analysis of films of the un-cross-linked **1·Eu(NTf$_2$)$_3$** and cross-linked **2a−c·Eu(NTf$_2$)$_3$**. Increased cross-linking results in a suppression of the T_g and mechanical enhancement above 40 °C at which point the un-cross-linked film flows as a result of disruption of the phase separated morphology.

linking density. In Figure 2b, the mechanical properties of the control film show two distinct transitions. The first is the T_g of the poly(butadiene) phase at ca. −60 °C, and the second occurs above 40 °C and relates to the disruption of the hard phase, which in turn causes the sample to yield/flow. As covalent cross-links are introduced to the poly(butadiene) core, both transitions are depressed, and above 50 °C the samples no longer flow and appear to approach a plateau region above 150 °C. In the lightly cross-linked film, a decrease in the storage modulus is still observed at T_g although not as much as the un-cross-linked sample. As the cross-linking increases, the T_g is replaced by a very broad and weak transition. The maximum for this transition is around 60 °C, after which the mechanical properties are predominantly a result of the permanent cross-linking. Not surprisingly, in general the modulus also increases with increasing cross-linking.

Thermally Induced Shape-Memory Properties. To deduce the shape-memory characteristics of these films, standard thermal shape-memory experiments using DMA were carried out. The strain-fixing ratio (R_f) and the strain-recovery ratio (R_r) are the most common values used to determine the efficiency of the

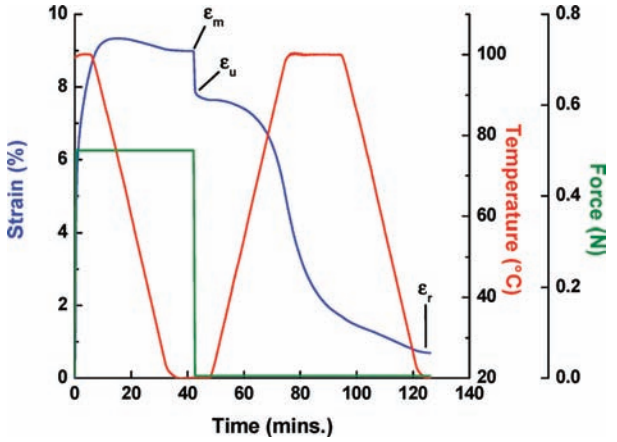

Figure 3. Standard thermal one-way shape-memory cycle for a film of **2a·Eu(NTf$_2$)$_3$**. The film is deformed at 100 °C to a set force, and the temperature is reduced while the force is held constant. The force is removed, and the strain fixing is determined. Heating the sample back to 100 °C followed by cooling to room temperature allows the material to recover its original shape.

shape-memory response.[52] The strain-fixing ratio is given as

$$R_f = \frac{\varepsilon_u}{\varepsilon_m} \times 100\% \quad (1)$$

where ε_m is the maximum strain after equilibration and ε_u is the strain after unloading, and the strain-recovery ratio is given as

$$R_r = \frac{\varepsilon_m - \varepsilon_r}{\varepsilon_m - \varepsilon_p} \times 100\% \quad (2)$$

where ε_r is the recovered strain and ε_p is the initial, permanent strain, which is set as 0 in the experiment. As the Eu^{3+}:ROMebip complex has been shown to be responsive to temperatures above 50 °C,[43] it stands to reason that these metallo-supramolecular polymer films should be able to thermally fix a temporary strain by heating above 50 °C, applying a fixed force to strain the material, and cooling below 50 °C before removing the force. Shape-memory would then be achieved by reheating the sample without any applied force. To determine the validity of this, films **2a−c·Eu(NTf$_2$)$_3$** were studied with a typical thermal one-way shape-memory cycle. An example result is shown in Figure 3 for **2a·Eu(NTf$_2$)$_3$** (results for films **2b·Eu(NTf$_2$)$_3$** and **2c·Eu(NTf$_2$)$_3$** can be found in the Supporting Information, S6,7). The sample was heated to 100 °C, and a 0.5 N force was applied. For the thermal shape-memory tests, forces above 0.5 N caused the samples to break when held at elevated temperatures for extended time periods. After being cooled to 25 °C, the load was removed, and the sample demonstrated fixing of the strained shape. Subsequent heating to 100 °C recovers the majority of the strain, and cooling back to 25 °C recovers the remaining strain that results from thermal expansion in the film. The initial strain fixing values (R_f) are high for all films **2a−c·Eu(NTf$_2$)$_3$** (87%, 87%, and 90%, respectively), and all show recovery values (R_r) above 90%, typically >97%. A video showing the thermally induced shape-memory behavior is available as part of the Supporting Information.

Light-Induced Shape-Memory Properties. Having demonstrated the thermal shape-memory properties of these materials, we went on to investigate their photoresponsive properties where we utilize the ability of the metal−ligand complexes to absorb light and convert some of that energy to localized heating.[45] An example of light-induced shape-memory behavior of a permanent shaped spiral of **2a·Eu(NTf$_2$)$_3$** is shown in Figure 4. The ability to trigger heating using UV light is interesting as it allows for remote activation of the shape-memory properties while also being able to control the response as the heating will be localized to only the areas exposed.

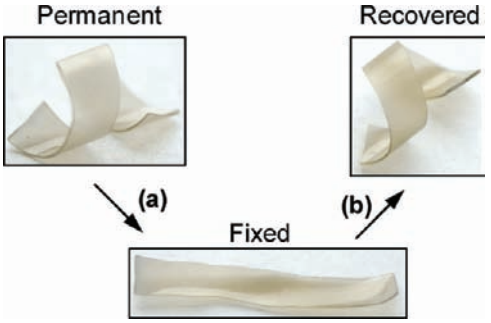

Figure 4. Images demonstrating the shape-memory behavior of a **2a·(EuNTf$_2$)$_3$** film. The film was set into a permanent spiral shape, (a) uncurled and irradiated with 320−390 nm UV light to fix the temporary shape and (b) irradiated with UV light to recover the permanent shape.

An example of the localized heating effect is shown in Figure 5. A **2b·Eu(NTf$_2$)$_3$** film displays the typical red Mebip:Eu^{3+} complex metal-based emission (Figure 5a) when observed under low intensity UV light (70 mW/cm^2). When the left side of the film is selectively irradiated with high intensity UV light (1000 mW/cm^2) (Figure 5b), the energy is converted into localized heating, which results in decomplexation of the Eu^{3+} that in turn converts the film to the blue, free Mebip emission. The red emission (as observed under low intensity light) returns over a period of a few seconds after removal of the high intensity light.

The shape-memory response using UV light as the stimulus was characterized by placing the samples in a DMA instrument and irradiating them with light. Films **2a−c·Eu(NTf$_2$)$_3$** were studied to elucidate the effect of cross-linking on the mechanical and shape-memory properties. A representative plot of the light-induced shape-memory behavior can be seen in Figure 5c. Controls were also performed without any exposure to UV light to act as a comparison. To prove that the mechanism for light-induced shape-memory behavior is a result of localized heating from absorbance of 320−390 nm UV light by the metal−ligand complexes and not from inadvertent heating from the light source, a **2b·Eu(NTf$_2$)$_3$** film was tested using the same conditions with a filter that blocks UV light below 400 nm (Supporting Information, S9). By doing this, the sample is still irradiated by the light source, but not in wavelengths absorbed by the metal−ligand hard phase. The film shows strains, fixing, and recovery values very similar to the nonirradiated controls, showing that there are little to no thermal effects from the light source and that the observed shape-memory behavior is a result of a photothermal conversion process. A video showing the light-induced shape-memory behavior is available as part of the Supporting Information.

The R_f and R_r values for the different cross-link density films are shown in Figure 6. All samples exposed to UV light display fixing values of over 80% of the deformed strain. This is a drastic improvement over the control films (which were strained and allowed to recover without exposure to light at room temperature)

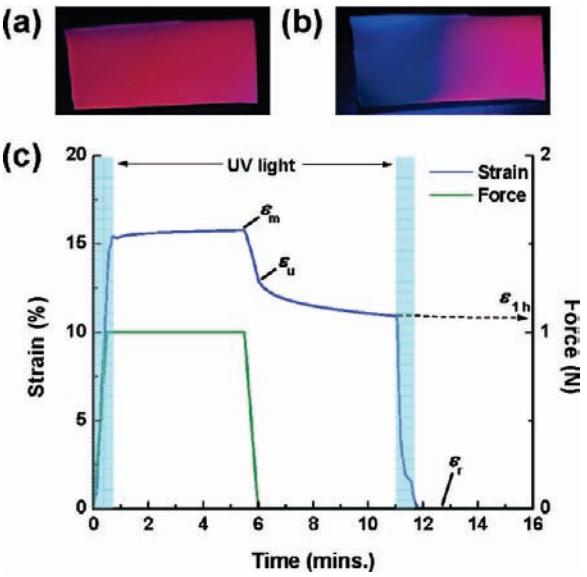

Figure 5. Picture of a cross-linked film of $\mathbf{2b \cdot Eu(NTf_2)_3}$ in its permanent shape (a) under low intensity (70 mW/cm^2) UV light and (b) selectively irradiating the left side of the film with high intensity (1000 mW/cm^2) UV light. (c) Typical controlled force shape-memory experiment on $\mathbf{2a \cdot Eu(NTf_2)_3}$. The sample was strained to a set force of 1 N while irradiated with light (UV light exposure of 30 s highlighted), allowed to equilibrate, and the force was removed to determine the initial shape fixing. Additional exposure to light removes the stored strain, and the sample returns to the permanent shape. (Shape-memory results for films of $\mathbf{2b \cdot Eu(NTf_2)_3}$ and $\mathbf{2c \cdot Eu(NTf_2)_3}$ can be found in the Supporting Information, S8 and 10.)

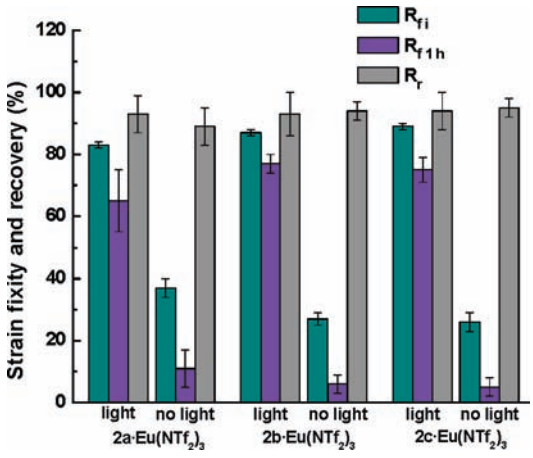

Figure 6. Strain fixing and recovery of films of $\mathbf{2a-c \cdot Eu(NTf_2)_3}$, which have different levels of permanent cross-link densities. Films exposed to light showed greatly increased strain-fixing over the nonirradiated control films while the recovery remained consistent for all. The dynamic nature of the reversible cross-links is responsible for the additional 10−15% decrease in the strain fixing 1 h after the initial unloading.

where fixing never exceeds 40%. The final recovered strain is >95% for both the irradiated samples and the controls, but the response time is much different. Samples irradiated with UV light show strain recovery in a matter of seconds, whereas the controls require approximately 1 h to completely recover. These initial

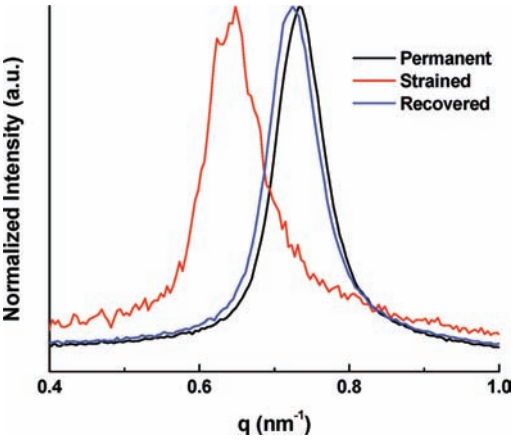

Figure 7. 1D SAXS of a film of $\mathbf{2a \cdot Eu(NTf_2)_3}$ in its permanent, strained, and recovered states. The peaks correspond to the distance between the "hard" metal−ligand phases and are 8.6 nm (permanent), 9.7 nm (strained), and 8.7 nm (recovered).

fixing and recovery values match well with those reported above for the thermally activated shape-memory behavior.

While R_f is typically defined using the strain immediately after unloading, this may not be the best way to report fixing values where the strain fixing is a result of a supramolecular interaction. Metal−ligand interactions are dynamic in nature, which is a result of constant complexation/decomplexation, even in the solid state. This can result in a slow recovery of the strain after the initial unloading. This is observable in Figure 5c between the unloading and recovery with light; however, it is apparent that the strain recovery decreases with time. Thus, it may be more accurate to describe R_f in terms of a fixing value after a given time period (ε_t) rather than the initial fixing after unloading. This new fixing value was determined by monitoring the strain recovery after unloading for 1 h, after which the strain was measured ($\varepsilon_{1\,h}$) and used in the place of ε_u as

$$R_{f\ 1\ h} = \frac{\varepsilon_{1\ h}}{\varepsilon_m} \times 100\% \qquad (3)$$

A comparison of the initial fixing values with the fixing after 1 h is also shown in Figure 6. After 1 h, the strain recovery of all films had slowed to less than 2.5 × 10^{-3} %/min, and the strain fixing for all $\mathbf{2a-c \cdot Eu(NTf_2)_3}$ films was still typically over 70% with the films having the lowest initial fixing also having the most strain recovery.

Figure 6 also shows that while the recovery stays relatively constant with cross-link density, the fixing increases in the higher cross-linked films. To further probe this effect, creep experiments were performed on each sample by straining the films using a 1 N set force without exposure to UV light and observing the strain increase over 30 min (see Supporting Information, S13). The rough creep rates were calculated as the increase in strain over 30 min under a 1 N load. All of the materials show a small amount of creep with the highest creep rate, 4.6 × 10^{-2} %/min (vs ca. 3.2 × 10^{-3} %/min for the highest cross-linked materials), being observed with the lowest cross-linked material. This is consistent with the soft phase not being fully cross-linked, which allows the materials to relax more after fixing.

The structural effects of straining, fixing, and recovering were also determined using SAXS. Figure 7 shows the primary Bragg diffraction peak for a film of $\mathbf{2a \cdot Eu(NTf_2)_3}$ in the permanent

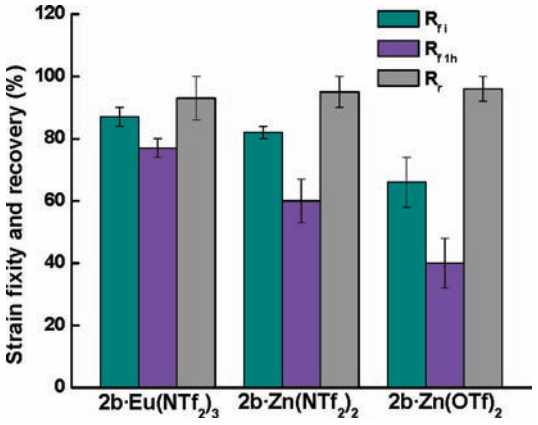

Figure 8. Strain fixing and recovery of films of **2b** with different metal salts. Recovery is unaffected by the metal salt used; however, the fixing value decreases when changing from europium to zinc and when the counterion is changed from $^{-}NTf_2$ to ^{-}OTf.

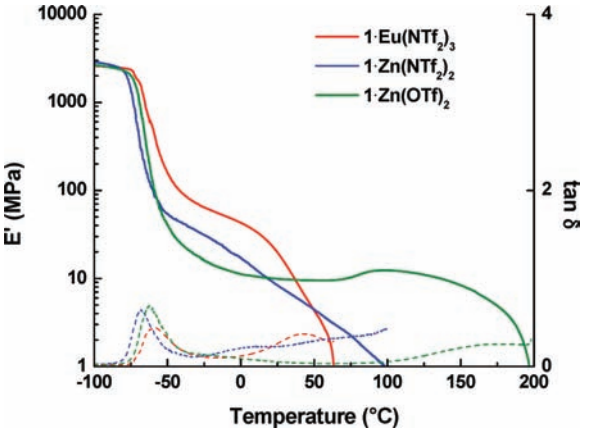

Figure 9. Dynamic mechanical thermal analysis of un-cross-linked films containing **1** with either $Eu(NTf_2)_3$, $Zn(NTf_2)_2$, or $Zn(OTf)_2$.

shape, after straining while irradiating with UV light to fix the temporary shape, and recovery after further irradiation. The film in its permanent shape has a peak corresponding to 8.6 nm as mentioned earlier, which is assigned to the distance between the metal−ligand "hard" phases. After straining the sample and fixing with light, the peak shifts to a smaller scattering vector (q), which relates to an increase in distance to ∼9.8 nm; however, this number is likely slightly exaggerated as orientation was observed in the 2D SAXS image for the strained film (see Supporting Information, S14). Further exposure with light results in recovery to 8.7 nm, which is essentially the value for the permanent shape. Thus, the SAXS confirms the changes in morphology during the shape-memory process are consistent with the process outlined in Figure 1.

Effect of Different Metals and Counterions on the Light-Induced Shape-Memory Behavior. In an effort to try to elucidate the role of the metal salt on the shape-memory properties, films were made in which the metal and/or counterion were varied. All films studied were prepared targeting 8 cross-links per chain. Films of **2b** with $Zn(NTf_2)_2$ and $Zn(OTf)_2$ (**2b·Zn(NTf$_2$)$_2$** or **2b·Zn(OTf)$_2$**) were prepared in the same manner as the $Eu(NTf_2)_3$ films, and their shape-memory behavior was studied to determine the influence of these metal salts on R_f and R_r.

Figure 8 shows the results of the shape-memory testing on the two zinc films (**2b·Zn(NTf$_2$)$_2$** or **2b·Zn(OTf)$_2$**) as compared to **2b·Eu(NTf$_2$)$_3$**. It is obvious that the metal and counterion have little to no effect on the recovery (R_r), as recovery is a result of the fixed phase (the cross-linked poly(butadiene)) restoring the stored strain. Changing the metal ion from Eu^{3+} to Zn^{2+} and keeping the counterion the same, however, results in a slight decrease in the initial fixing of approximately 5% and an even bigger decrease in the fixing value over 1 h (only ca. 60% fixing vs 77% for **2b·Eu(NTf$_2$)$_3$**). This result is consistent with the inability to achieve full decomplexation of the Zn^{2+} from the ligand during exposure to UV light, presumably as a result of more energy being required to disrupt the more strongly bound phase separated zinc complexes as compared to those with europium. Changing the counterion from bistriflimide to triflate results in a much more dramatic decrease in the fixing values. There is approximately a 16% decrease in the initial fixing value comparing the films made with $Zn(OTf)_2$ to $Zn(NTf_2)_2$ and a 21% decrease when compared to the $Eu(NTf_2)_3$ film. The fixing values are even more dramatic after 1 h, with **2b·Zn(OTf)$_2$** exhibiting a fixing value of only 40%. This result implies that the counterion has a large influence on the packing of the "hard" metal−ligand phase and that by changing from a bulky bistriflamide to a triflate counterion, much higher temperatures are necessary to disrupt the phase separation. Thus, for the given exposure time, only partial disruption of the reversible phase occurs, and the metal−ligand complexes that are not broken now act with the covalent cross-links to recover the strain. This means that the initial fixing value also reflects the recovery rate after 1 h where films with higher initial fixing values have slower strain recovery with time.

To further probe the effect the metal salts have on the properties of these materials, the mechanical properties of un-cross-linked films of **1** with $Eu(NTf_2)_3$, $Zn(NTf_2)_2$, and $Zn(OTf)_2$ were explored. As shown in Figure 9, the films display very different thermal behavior. At temperatures above T_g of the poly(butadiene) core, the mechanical properties are primarily a result of the phase separated morphology between the hard metal−ligand complexes and the soft polymer core. Once a temperature is achieved that is sufficient to induce a breakup of the metal−ligand hard phase and an increase in metal−ligand decomplexation rate, the material will flow. Figure 9 shows that for the $Eu(NTf_2)_3$ film, the temperature required to disrupt the phase separation is only slightly above room temperature, with the materials flowing above 40 °C. Conversely, the $Zn(OTf)_2$ films, while having slightly lower modulus values, are mechanically stable above 150 °C, and thus much higher temperatures must be achieved to disrupt the phase separation. This dramatic change in thermal stability of these metallo-supramolecular films with different metal salts is probably related to the T_g (or T_m) and/or order−disorder transition of the resulting metal−ligand hard phase in the soft polymer matrix, although we have not been able to definitively identify such a thermal transition in differential scanning calorimetric (DSC) studies of these materials. Nevertheless, these results are consistent with the degree of fixing in the shape-memory materials being related to the thermal stability of the hard phase, which in turn is controlled by the different metals and counterions.

Localized Shape-Memory Response. As mentioned earlier, light-activated systems are advantageous as they offer the possibility of producing a localized shape-memory response.

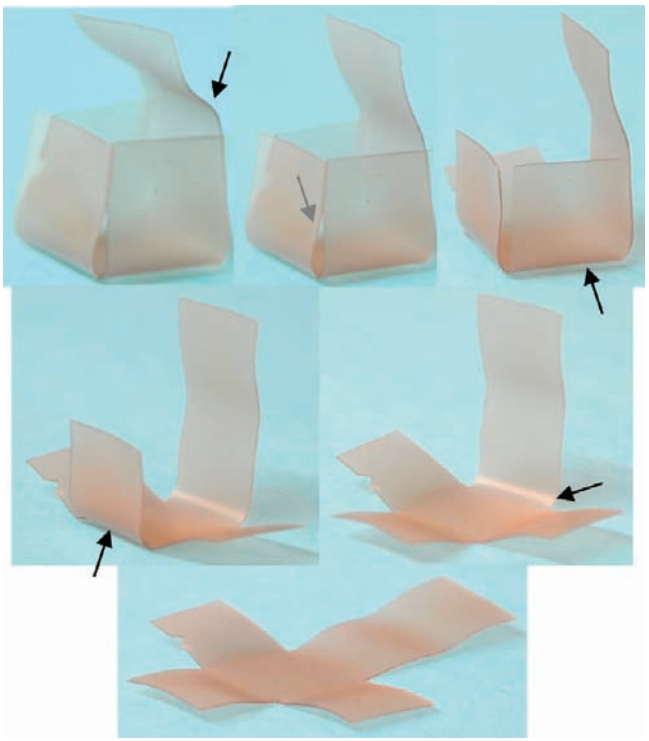

Figure 10. Demonstration of the localized shape-memory effect in films of $\mathbf{2b \cdot Eu(NTf_2)_3}$. Using UV light, films can be fixed into complex shapes such as a box. The sides of the box can then be selectively opened by irradiating at the apex (shown with arrows) to return to the permanent shape.

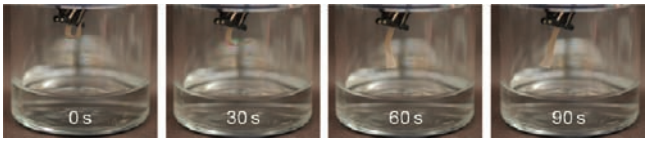

Figure 11. Demonstration of chemo-responsive shape-memory behavior. A $\mathbf{2b \cdot Eu(NTf_2)_3}$ film was fixed into a bent shape using UV light and suspended above methanol in a sealed container. Methanol affects the stability of the metal–ligand complexes, which results in decreased phase separation that leads to recovery of the permanent shape.

To demonstrate this, we prepared a 1 cm^3 cube from a $\mathbf{2b \cdot Eu(NTf_2)_3}$ film. The permanent, "remembered" shape is a cross template, and by folding each side and irradiating with UV light, a 3D box temporary shape was obtained as shown in Figure 10. Irradiating the top edge only allows the box top to open while the sides maintain their temporary shape. Figure 10 shows the result of selectively irradiating each of the vertices of the box, one at a time, to open each side of the box until the box has returned to its permanent cross template. The localization effect is only limited by the size of the UV light source and could be expected to work on much smaller scales, which would be useful for a variety of applications.

Chemo-Responsive Shape-Memory Effect. The data suggest that the thermal stability of the metal–ligand hard phase is critical to the shape-memory properties of these films. Therefore, conceptually any chemical that can impact the thermal stability of this hard phase (e.g., via plasticization or decomplexation of the metal–ligand complex) could be used to induce shape-memory properties. Thus, we examined the potential of a few solvents to induce recovery of the permanent shape of a $\mathbf{2b \cdot Eu(NTf_2)_3}$ film. The film, which had a permanent rectangular shape, was initially fixed using light, as described earlier, to bend the film in half. The temporarily fixed film was suspended in a sealed container above the appropriate solvent. Figure 11 shows the effect of a methanol atmosphere on the film. After only 2 min of exposure, the film showed near full recovery back to the permanent shape. Films of $\mathbf{2b \cdot Zn(NTf_2)_2}$ and $\mathbf{2b \cdot Zn(OTf)_2}$ also showed shape recovery when exposed to a methanol environment. Taken together, these results are more consistent with the methanol plasticizing the metal–ligand hard phase rather than a competitively binding process as the Bip:Zn^{2+} complexes are stable in the presence of alcohols.[53] The film also showed some shape-memory behavior when exposed to other chemicals such as acetone and triethylamine; however, samples exposed to triethylamine display only partial shape-recovery and discoloration resulting from oxidation. As a result, we were able to demonstrate a third shape-memory stimulus for these films in the form of chemo-responsiveness.

CONCLUSIONS

Utilizing a metallo-supramolecular polymer with a covalently cross-linkable core, shape-memory films have been made. We used a covalent photo-cross-linking process wthat allows the possibility of accessing complex permanent shapes and a metal–ligand hard phase as the reversible phase used to fix the temporary shape. Therefore, any stimulus (thermo-, photo-, and chemo-) that results in softening of the hard phase and increased decomplexation or rate of exchange of the metal–ligand complexes can be used to access the shape-memory properties of these films. In addition, the low thermal conductivity of the polymer allows light to selectively target a localized shape-memory response of the temporary shapes. Varying cross-link densities of the soft phase were studied, and all were found to have excellent shape-memory properties with initial strain-fixing values greater than 80% and strain-recovery over 95%. Finally, the use of different metal salts, which impact the properties of the hard phase, allows the fixing behavior of these materials to be tailored. Thus, we have demonstrated that a combination of dynamic metal–ligand complexes phase separated into a hard phase is a flexible platform with which to create shape-memory materials that have the ability to respond to multiple stimuli.

ASSOCIATED CONTENT

Supporting Information. NMR, mass spectroscopy, and UV–vis characterization of the macromonomer **1**; thermal shape-memory cycles and light-induced shape-memory curves of $\mathbf{2b \cdot Eu(NTf_2)_3}$ and $\mathbf{2c \cdot Eu(NTf_2)_3}$; creep rates versus cross-link density of $\mathbf{2a–c \cdot Eu(NTf_2)_3}$; 2D SAXS pattern of $\mathbf{2a \cdot Eu(NTf_2)_3}$; and DMA of $\mathbf{2b \cdot Zn(NTf_2)_2}$ and $\mathbf{2b \cdot Zn(OTf)_2}$ films. This material is available free of charge via the Internet at http://pubs.acs.org.

AUTHOR INFORMATION

Corresponding Author
stuart.rowan@case.edu

■ ACKNOWLEDGMENT

This material is based upon work supported by the National Science Foundation under Grant nos. CHE-0704026 and MRI-0821515 (for the purchase of the MALDI-TOF/TOF) and by the Case School of Engineering and the Kent H. Smith Charitable Trust. We would also like to thank Brian Michal for help with the SAXS experiments

■ REFERENCES

(1) Behl, M.; Razzaq, M. Y.; Lendlein, A. *Adv. Mater.* **2010**, *22* 3388–3410.
(2) Lendlein, A.; Shastri, V. P. *Adv. Mater.* **2010**, *22*, 3344–3347.
(3) Ratna, D.; Kocsis, J. K. *J. Mater. Sci.* **2008**, *43*, 254–269.
(4) Liu, C.; Qin, H.; Mather, P. T. *J. Mater. Chem.* **2007**, *17*, 1543–1558.
(5) Small, W., IV; Metzger, M. F.; Wilson, T. S.; Maitland, D. J. *IEEE J. Sel. Top. Quantum Electron.* **2005**, *11*, 892–901.
(6) Sokolowski, W.; Metcalfe, A.; Hayashi, S.; Yahia, L.; Raymond, J. *Biomed. Mater.* **2007**, *2*, S23–S27.
(7) Buckley, P. R.; McKinley, G. H.; Wilson, T. S.; Small, W., IV; Benett, W. J.; Bearinger, J. P.; McElfresh, M. W.; Maitland, D. J. *IEEE Trans. Bio-Med. Electron.* **2006**, *53*, 2075–2083.
(8) Small, W., IV; Wilson, T. S.; Benett, W. J.; Loge, J. M.; Maitland, D. J. *Opt. Express* **2005**, *13*, 8204–8213.
(9) Meng, Q. H.; Hu, J. L.; Zhu, Y.; Lu, J.; Liu, Y. *Smart Mater. Struct.* **2007**, *16*, 1192–1197.
(10) Meng, Q. H.; Hu, J. L. *Composites, Part A* **2009**, *40*, 1661–1672.
(11) Mather, P. T.; Luo, X.; Rousseau, I. A. *Annu. Rev. Mater. Res.* **2009**, *39*, 445–471.
(12) Ahn, S.; Deshmukh, P.; Kasi, R. M. *Macromolecules* **2010**, *43*, 7330–7340.
(13) Zhou, J.; Schmidt, A. M.; Ritter, H. *Macromolecules* **2010**, *43*, 939–942.
(14) Ishida, K.; Yoshie, N. *Macromolecules* **2008**, *41*, 4753–4757.
(15) Jiang, H.; Kelch, S.; Lendlein, A. *Adv. Mater.* **2006**, *18*, 1471–1475.
(16) Yu, Y.; Ikeda, T. *Macromol. Chem. Phys.* **2005**, *206*, 1705–1708.
(17) Chen, M.; Xing, X.; Liu, Z.; Zhu, Y.; Liu, H.; Yu, Y.; Cheng, F. *Appl. Phys. A: Mater. Sci. Process.* **2010**, *100*, 39–43.
(18) Leng, J.; Zhang, D.; Liu, Y.; Yu, K.; Lan, X. *Appl. Phys. Lett.* **2010**, *96*, 111905/1–111905/3.
(19) Lendlein, A.; Jiang, H.; Jünger, O.; Langer, R. *Nature* **2005**, *434*, 879–882.
(20) Leng, J.; Wu, X.; Liu, Y. *J. Appl. Polym. Sci.* **2009**, *114*, 2455–2460.
(21) Koerner, H.; Price, G.; Pearce, N. A.; Alexander, M.; Vaia, R. A. *Nat. Mater.* **2004**, *3*, 115–120.
(22) Weigel, T.; Mohr, R.; Lendlein, A. *Smart Mater. Struct.* **2009**, *18*, 1–9.
(23) Yakacki, C. M.; Satarkar, N. S.; Gall, K.; Likos, R.; Hilt, J. Z. *J. Appl. Polym. Sci.* **2009**, *112*, 3166–3176.
(24) Leng, J.; Lan, X.; Liu, Y.; Du, S. *Prog. Mater. Sci.* **2011**, *56*, 1077–1135.
(25) Huang, W. M. *Open Med. Devices J.* **2010**, *2*, 11–19.
(26) Lu, H.; Liu, Y.; Leng, J.; Du, S. *Smart Mater. Struct.* **2009**, *18*, 1–5.
(27) For some examples of other materials that use reversible metal−ligand coordination to access stimuli-responsive systems, see: (a) Paulusse, J. M. J.; van Beek, D. J. M.; Sijbesma, R. P. *J. Am. Chem. Soc.* **2004**, *126*, 15802–15808. (b) Yount, W. C.; Loveless, D. M.; Craig, S. L. *J. Am. Chem. Soc.* **2005**, *127*, 14488–14496. (c) Kim, H.-J.; Lee, J.-H.; Lee, M. *Angew. Chem., Int. Ed.* **2005**, *44*, 5810–5814. (d) South, C. R.; Pinon, V.; Weck, M. *Angew. Chem., Int. Ed.* **2008**, *47*, 1425–1428. (e) Xu, D. H.; Liu, C. Y.; Craig, S. L. *Macromolecules* **2011**, *44*, 2343–2353. (f) Nair, K.; Breedveld, V.; Weck, M. *Macromolecules* **2011**, *44*, 3346–3357.
(28) Han, S.-I.; Gu, B. H.; Nam, K. H.; Im, S. J.; Kim, S. C.; Im, S. S. *Polymer* **2007**, *48*, 1830–1834.
(29) Guan, Y.; Cao, Y.; Peng, Y.; Xu, J.; Chen, A. S. C. *Chem. Commun.* **2001**, 1694–1695.
(30) Weiss, R. A.; Izzo, E.; Mandelbaum, S. *Macromolecules* **2008**, *41*, 2978–2980.
(31) Merline, J. D.; Nair, C. P. R.; Gouri, C.; Shrisudha, T.; Ninan, K. N. *J. Mater. Sci.* **2007**, *42*, 5897–5902.
(32) Zhang, S.; Yu, Z.; Govender, T.; Luo, H.; Li, B. *Polymer* **2008**, *49*, 3205–3210.
(33) Chen, S.; Hu, J.; Zhuo, H.; Yuen, C.; Chan, L. *Polymer* **2010**, *51*, 240–248.
(34) Chen, S.; Hu, J.; Liu, Y.; Liem, H.; Zhu, Y.; Liu, Y. *J. Polym. Sci., Part B: Polym. Phys.* **2007**, *45*, 444–454.
(35) Chen, S.; Cao, Q.; Jing, B.; Cai, Y.; Liu, P.; Hu, J. *J. Appl. Polym. Sci.* **2006**, *102*, 5224–5231.
(36) Li, J.; Viveros, A.; Wrue, M. H.; Anthamatten, M. *Adv. Mater.* **2007**, *19*, 2851–2855.
(37) Kushner, A. M.; Vossler, J. D.; Williams, G. A.; Guan, Z. *J. Am. Chem. Soc.* **2009**, *131*, 8766–8768.
(38) Fox, J. D.; Rowan, S. J. *Macromolecules* **2009**, *42*, 6823–6835.
(39) Wojtecki, R. J.; Meador, M. A.; Rowan, S. J. *Nat. Mater.* **2011**, *10*, 14–27.
(40) Hsu, L.; Weder, C.; Rowan, S. J. *J. Mater. Chem.* **2011**, *21*, 2812–2822.
(41) Whittell, G. R.; Hager, M. D.; Schubert, U. S.; Manners, I. *Nat. Mater.* **2011**, *10*, 176–188.
(42) Dobrawa, R.; Würthner, F. *J. Polym. Sci., Part A: Polym. Chem.* **2005**, *43*, 4981–4995.
(43) Kumpfer, J. R.; Jin, J.; Rowan, S. J. *J. Mater. Chem.* **2010**, *20*, 145–151.
(44) Knapton, D.; Burnworth, M.; Rowan, S. J.; Weder, C. *Angew. Chem., Int. Ed.* **2006**, *45*, 5825–5829.
(45) Burnworth, M.; Tang, L.; Kumpfer, J. R.; Duncan, A. J.; Beyer, F. L.; Fiore, G. L.; Rowan, S. J.; Weder, C. *Nature* **2011**, *472*, 334–337.
(46) Kade, M. J.; Burke, D. J.; Hawker, C. J. *J. Polym. Sci., Part A: Polym. Chem.* **2010**, *48*, 743–750.
(47) Nie, J.; Kobayashi, H.; Sonoda, T. *Catal. Today* **1997**, *36*, 81–84.
(48) Beck, J. B.; Rowan, S. J. *Faraday Discuss.* **2005**, *128*, 43–53.
(49) Beck, J. B.; Ineman, J. M.; Rowan, S. J. *Macromolecules* **2005**, *38*, 5060–5068.
(50) (a) Lis, S. *J. Alloys Compd.* **2002**, *341*, 45–50. (b) Sabbatini, N.; Guardigli, M.; Lehn, J.-M. *Coord. Chem. Rev.* **1993**, *123*, 201–228.
(51) Petoud, S.; Bünzli, J.-C. G.; Glanzman, T.; Piguet, C.; Xiang, Q.; Thummel, P. *J. Lumin.* **1999**, *82*, 69–79.
(52) Lendlein, A.; Kelch, S. *Angew. Chem., Int. Ed.* **2002**, *41*, 2034–2057.
(53) Weng, W.; Li, Z.; Jamieson, A. M.; Rowan, S. J. *Macromolecules* **2009**, *42*, 236–246.